Chemistry & Biodiversity

WILEY-VCH

CHEMISTRY & BIODIVERSITY

RESEARCH ARTICLE

Bioactive Compounds From *Rosa canina* L. Roots With Anti-Collagenase, Anti-Tyrosinase, and Antioxidant Activities: In Vitro and In Silico Approaches

Tuğba Subaş[1] | Ufuk Özgen[1] | Şeyda Kanbolat[2] | Merve Badem[2] | Uğur Uzuner[3] | Gonca Özdemir[1] | Şule Zeytineli[1] | Şeyma Altunışık[1] | Halide Cangul[1] | Özgür Eminağaoğlu[4]

[1]Department of Pharmacognosy, Faculty of Pharmacy, Karadeniz Technical University, Trabzon, Türkiye | [2]Department of Biochemistry, Faculty of Pharmacy, Karadeniz Technical University, Trabzon, Türkiye | [3]Department of Molecular Biology and Genetics, Faculty of Science, Karadeniz Technical University, Trabzon, Türkiye | [4]Department of Forest Engineering, Faculty of Forestry, Artvin Çoruh University, Artvin, Türkiye

Correspondence: Şeyda Kanbolat (seydaakkaya@ktu.edu.tr)

Received: 27 January 2025 | **Revised:** 24 May 2025 | **Accepted:** 27 May 2025

Funding: This study was funded by The Scientific and Technological Research Council of Türkiye (TUBITAK) (Grant Number: 1919B012337704) and Office of Scientific Research Projects of Karadeniz Technical University (Grant Number: TLÖ-2023-11098).

Keywords: cosmetic | isolation | molecular docking | Rosaceae | SwissADME

ABSTRACT

The study aimed to investigate the anti-aging, skin-whitening, and antioxidant capacities of the extracts and constituents from the roots of *Rosa canina* L. by anti-collagenase, anti-tyrosinase activity, ferric-reducing antioxidant power (FRAP), cupric-reducing antioxidant capacity (CUPRAC) assays, and the Folin–Ciocalteu method (for the extracts). Enzyme inhibitory activities, pharmacokinetics, and drug-likeness properties of the compounds were evaluated in silico. According to the results of activity studies, the ethyl acetate subextract exhibited the highest anti-tyrosinase activity, and the remaining aqueous subextract demonstrated the highest anti-collagenase activity. The isolation studies led to the purification of euscaphic acid (**1**), tormentic acid (**2**), kaji-ichigoside F1 (**3**), rosamultin (**4**), 2-oxopomolic acid (**5**), and (+)-catechin (**6**) for the first time from the roots of this plant. Isolated compounds exhibited anti-collagenase and anti-tyrosinase activities. The extracts and (+)-catechin had higher antioxidant capacities than other compounds. *R. canina* roots and their compounds can be included in dermocosmetic products after further studies.

1 | Introduction

The genus *Rosa* (Rosaceae), widely used as a fragrant and ornamental plant, is represented by 278 species worldwide and 31 in Türkiye [1, 2]. *Rosa canina* L., which grows naturally in Europe, Northwest Africa, and Western Asia, is known in Türkiye by names such as "kuşburnu, gül, itburnu, yabani gül, köpek gülü, gül elması, ip burması" [3, 4]. Different parts of *R. canina* are used in folk medicine, and its roots are used for colds, bronchitis, asthma, throat cancer, hemorrhoids, infertility, diabetes, and rheumatism, and to pass kidney stones, and also as a tonic, diuretic, stomachic, and immunostimulant. Although more studies have been conducted on the fruits of the species, the phytochemical and pharmacological evaluation of its roots is limited. Macit et al. [6] investigated the antioxidant capacity of the methanol extract of *R. canina* roots together with characterizing some phenolic compounds such as catechin, epicatechin, gallic acid, syringic acid, *p*-coumaric acid, 4-hydroxybenzoic acid, ellagic acid, naringenin and quercetin by high-performance liquid chromatography-photodiode array detector (HPLC-PDA).

They also determined that the phenolic content of the methanol extract of the roots was higher than the methanol extract of the fruits. Deliorman Orhan et al. [7] conducted a study on decoctions prepared from different parts of *R. canina* and concluded that the total phenolic content of the roots was higher than that of the leaves, shoots, and flowers of the plant.

The skin, the largest organ of the body, consists of three parts: epidermis, dermis, and hypodermis, and protects the body from external factors [8]. The extracellular matrix of the dermis layer contains collagen, which provides resistance to the skin [9]. The skin aging process occurs under the influence of internal (age, genetics) and external factors (lifestyle components, environmental factors, chronic exposure to ultraviolet [UV] rays, oxidative stress) that cause significant changes in skin structure and elasticity [10, 11]. Reactive oxygen species (ROS) formed in the skin as a result of continuous exposure to UV rays, especially sunlight, cause oxidative stress and inflammatory responses, and photoaging occurs [11, 12]. Due to excessive ROS exposure, the expression of collagenase, a matrix metalloproteinase that breaks down collagen, increases, resulting in decreased skin durability, wrinkles, and sagging [9, 13]. In addition, tyrosinase, a rate-limiting enzyme that has a copper-containing center and is involved in the conversion of tyrosine to melanin, catalyzes the reactions of hydroxylation of tyrosine and its conversion to *o*-quinones. Overproduction of melanin causes skin discoloration, hyperpigmentation, and skin aging. Therefore, tyrosinase inhibition is targeted for skin whitening, and agents that inhibit this enzyme are included in the composition of cosmetic products [10, 14]. On the other hand, defense systems against free radicals are weakened in aged skin, and antioxidant substances are preferred to reduce skin damage due to their free radical scavenging activities [15, 16].

Plants, plant extracts, and secondary metabolites obtained from plants are widely used for cosmetic purposes owing to their antiaging, skin-whitening, sun protection, moisturizing, anti-wrinkle, anti-acne, and antioxidant activities [17]. Natural antioxidant compounds such as arbutin, retinol, polyphenols, hydroquinone, vitamin C, α-lipoic acid, and niacinamide used in the cosmetic industry can suppress melanogenesis and regulate the extracellular matrix, but their effectiveness is controversial due to their insufficient penetration into the skin and instability [9, 13]. Investigations are still ongoing to find more effective and safe new active compounds or extracts that show collagenase and tyrosinase enzyme inhibitory activities to prevent skin aging and can especially prevent UV-induced oxidative damage.

Catechins prevent the deterioration of the extracellular matrix caused by UV radiation and other factors and have significant free radical scavenging activity [18]. Triterpenes (aglycone and saponins) are surface-active substances and show anti-inflammatory, antioxidant, and antibacterial activities [19]. Phenolic compounds have sun protection, anti-aging, and anti-inflammatory activities [20, 21]. Therefore, these secondary metabolites have significant potential for cosmetic applications. Studies have shown that the roots of *Rosa* sp. are rich in catechins, phenolic acids, and triterpenes [13, 22]. In this context, we preferred *R. canina* roots, which are widely distributed in Türkiye, to evaluate its cosmetic potential.

This study aimed to evaluate the effects of *R. canina* roots and their major compounds against some skin disorders and their usability in cosmetics. In this context, antioxidant capacity, and collagenase, tyrosinase enzyme inhibitory activities of the isolated compounds and the extracts from the roots were investigated. In addition, the total phenolic content of the extracts was determined. The interactions of the isolated compounds with the specified enzymes were revealed by in silico methods. The pharmacokinetic and drug-likeness properties of the isolated compounds were also investigated.

2 | Results and Discussion

2.1 | Isolation of the Major Compounds

In this study, enzyme inhibitory (collagenase and tyrosinase) and antioxidant activities of the roots of *R. canina* and its isolated compounds, as well as the total phenolic content of the extracts, were investigated. For this purpose, the extracts of the root's increasing polarity were prepared using the liquid–liquid partition method with different solvents, and the isolation studies were carried out on the subextracts prepared from the methanol extract (RCM) to obtain the major compounds. The chloroform subextract (RCC) and ethyl acetate subextract (RCE) were applied to various chromatographic methods, which led to the isolation of two compounds (ursane-type triterpene aglycones) and four compounds (two ursane-type triterpene glycosides, one aglycone, and one flavan-3-ol), respectively. The compounds were identified as euscaphic acid (**1**) [23], tormentic acid (**2**) [23], kaji-ichigoside F1 (**3**) [24], rosamultin (**4**) [24], 2-oxopomolic acid (**5**) [25], and (+)-catechin (**6**) [26] by the comparison of the spectroscopic data with the published data (Figure 1). Nuclear magnetic resonance (NMR) data of the compounds are presented in Supporting Information. Although these compounds have been purified from other *Rosa* species before, they have been reported from the roots of this species. In previous studies, tormentic acid, kaji-ichigoside F1, euscaphic acid and rosamultin from the roots of *Rosa rugosa*, *Rosa cymosa*, and *Rosa laevigata* [27–29]; 2-oxopomolic acid, euscaphic acid, and tormentic acid from *Rosa roxburghii* [30], and catechin from the roots of *Rosa heckeliana* [26] have been obtained. In this study, after evaluating the activity of the extracts, the isolated compounds were further tested to investigate their contribution to the activity.

2.2 | Inhibitory Effects of the Extracts and Isolated Compounds on Collagenase and Tyrosinase Enzymes

Collagen, the most important component of the skin's extracellular matrix, is responsible for providing skin strength and elasticity. The degradation of collagen as a result of exposure to UV light is responsible for the aging process [20]. All test samples revealed collagenase inhibitory activity, and IC_{50} values are presented in Table 1. The remaining aqueous subextract (RCA) (IC_{50} = 60.710 ± 3.437 μg/mL) and RCM (IC_{50} = 62.450 ± 4.245 μg/mL) were the most effective extracts in terms of collagenase inhibition. They may have higher activity thanks to their phenolic compounds. It is recorded in the literature that phenolic compounds (ferulic acid, caffeic

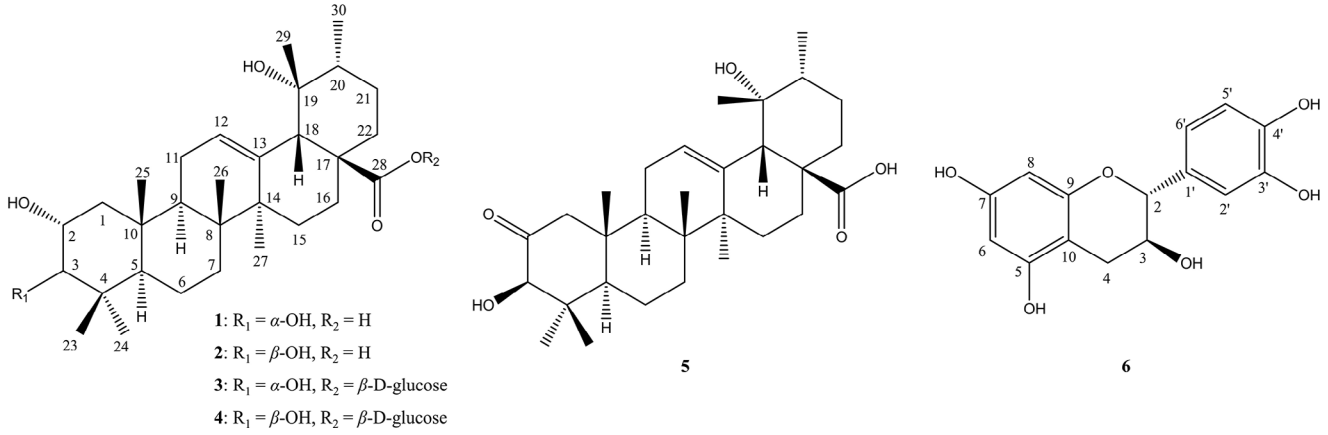

FIGURE 1 | Structures of the isolated compounds from the roots of *Rosa canina*.

acid, etc.) cause significant collagenase inhibition [31]. (+)-Catechin (IC_{50} = 53.285 ± 2.522 μg/mL) and euscaphic acid (IC_{50} = 55.743 ± 2.658 μg/mL) had similar IC_{50} values and showed higher activity than the other compounds. Catechin is used as a reference compound in collagenase inhibition studies, and catechin isolated from the roots had the highest activity in this study. Green tea and its catechins are included in the composition of topical products with anti-aging effects [32]. In a study fixed on the data that green tea catechins are protease inhibitors, the infusion prepared from white tea has been found to have significant collagenase inhibition [33]. It has been reported that catechin and other polyphenolic compounds in green tea inhibit the enzyme by binding to zinc in the enzyme due to their metal-chelating properties [34]. In addition, Madhan et al. [35] determined that the conformational change made by green tea catechins causes *Clostridium histolyticum* collagenase I inhibition, and catechin shows a competitive inhibition mode to the enzyme. On the other hand, euscaphic acid exhibited a significant activity very close to catechin. To our knowledge, no studies have been found on the collagenase inhibitory activities of the isolated triterpenes in this study. In a study examining the extracts of *Isodon rugosus* produced in vitro callus culture, it was concluded that the pentacyclic triterpenoid content of the extracts was associated with collagenase and tyrosinase inhibition [36].

All tested extracts and isolated compounds were observed to have tyrosinase inhibitory effects. RCE (IC_{50} = 21.767 ± 3.890 μg/mL) was the most effective extract and was found to be more active than the isolated compounds and the standard compound. The high activity may be owing to the synergistic effect of the major compounds isolated from this subextract and its other compounds. Euscaphic acid (IC_{50} = 36.597 ± 1.008 μg/mL) was the most active compound and showed an activity quite close to α-kojic acid. In a study, euscaphic acid had significant tyrosinase enzyme inhibitory activity (IC_{50} = 0.95 ± 0.11 mM, α-kojic acid: 0.41 ± 0.02 mM) [37] and this result supports our findings. In the literature, cell culture studies on hyperpigmentation have shown that compounds may have different mechanisms of action other than tyrosinase inhibitory activity. In a study, the effects of 2-oxopomolic acid and euscaphic acid on melanogenesis in B16-F10 melanoma cells were determined by comparing them with α-arbutin. It was found that euscaphic acid inhibited melanogenesis more than α-arbutin and 2-oxopomolic acid inhibited melanogenesis similar to α-arbutin without causing toxicity in the cell [25]. In another study, B16-F10 melanoma cells stimulated with α-MSH were used, 70% ethanol extract and *n*-butanol fractions of the branches of *Sorbus alnifolia* inhibited cellular melanogenesis and intracellular tyrosinase activities in a concentration-dependent manner without causing cell toxicity. 2-Oxopomolic acid and euscaphic acid were isolated as compounds responsible for the effect of the active fractions [38]. The anti-melanogenesis effect of tormentic acid was investigated in B16 cells and it was determined that it selectively inhibited melanogenesis (selectivity index > 1, IC_{50} = 18.5 μM) [39].

It is possible to explain the structure–activity relationships of the isolated pentacyclic triterpenes for the enzyme inhibitory activities. In the inhibition of both enzymes, glycosylation of the —COOH group at C-17 and the —oxo group at C-2 decreased the activity. When aglycone compounds (euscaphic acid and tormentic acid) were compared for collagenase inhibition, the presence of the —OH group at C-3 at the α position increased the activity. Although the opposite was the case for glycosides (kaji-ichigoside F1 and rosamultin), the activities were found to be close. In tyrosinase inhibition, the presence of the —OH group at C-3 at the α position in aglycones and glycosides is associated with higher activity. Similar to our findings, a study examining the structure–activity relationships of pentacyclic triterpenes isolated from *Rhododendron collettianum* reported that the inhibitory effect against tyrosinase enzyme increased when the position of the —OH group at the C-3 was changed from β to α, and the activity decreased with the esterification of the —COOH group at the C-17 [40].

2.3 | Antioxidant Activities of the Extracts and Isolated Compounds

Skin aging and various skin diseases may occur due to lipid peroxidation, DNA mutation, and membrane damage resulting from oxidative damage. The skin reacts with free radicals formed through the antioxidant defense mechanism [41]. In this study, the antioxidant capacities of the samples were expressed as Trolox equivalent antioxidant capacity (TEAC) (Table 2). In the FRAP assay, RCC (1796.733 ± 3.859 μM Trolox equivalent [TE]/g) and in the CUPRAC assay, RCE (930.000 ± 0.900 μM TE/g) were the

TABLE 1 | Enzyme inhibitory activities of the extracts and isolated compounds of the roots of *Rosa canina*.

Test compounds	Inhibition of enzymes (IC_{50} values, μg/mL)	
	Collagenase	Tyrosinase
RCM	62.45 ± 4.25	55.29 ± 1.33
RCC	186.11 ± 6.56	60.12 ± 9.96
RCE	114.87 ± 6.73	21.77 ± 3.89
RCA	60.71 ± 3.44	62.86 ± 3.90
1	55.74 ± 2.66	36.60 ± 1.01
2	72.34 ± 3.20	53.56 ± 2.38
3	89.08 ± 2.18	85.30 ± 1.33
4	82.94 ± 5.90	111.98 ± 11.98
5	85.39 ± 2.31	79.71 ± 6.24
(+)-Catechin[a]	53.29 ± 2.52	49.13 ± 7.77
α-Kojic acid[a]	—	33.05 ± 1.67

[a]Reference compounds.

TABLE 2 | FRAP and CUPRAC values of the extracts and isolated compounds and TPC values of the extracts of the roots of *Rosa canina*.

Test compounds	FRAP	CUPRAC	TPC
RCM	1471.40 ± 4.08	813.61 ± 1.09	639.96 ± 3.28
RCC	1796.73 ± 3.86	479.44 ± 2.05	134.54 ± 2.57
RCE	1623.40 ± 2.94	930.00 ± 0.90	582.46 ± 5.98
RCA	1714.73 ± 3.40	697.36 ± 3.57	698.71 ± 3.68
1	22.07 ± 1.89	67.22 ± 0.81	—
2	81.40 ± 1.63	48.47 ± 2.58	—
3	247.07 ± 3.09	18.19 ± 1.04	—
4	89.07 ± 4.11	17.64 ± 1.29	—
5	104.73 ± 2.49	105.83 ± 2.23	—
6	1711.73 ± 0.96	1044.03 ± 1.04	—

Abbreviations: CUPRAC, copper-reducing antioxidant power (μM Trolox equivalent/g); FRAP, iron-reducing antioxidant power (μM Trolox equivalent/g); TPC, total phenolic content (μg GAE/mL).

TABLE 3 | Molecular docking outputs of the studied compounds and predicted K_i values of collagenase G inhibition.

Ligand ID	7Z5U Binding energy (kcal/mol)	Estimated K_i (nM)	Ligand efficiency	H bond number
1	−9.12	206.54	−0.26	3
2	−8.76	379.21	−0.26	3
3	−8.81	348.53	−0.19	3
4	−8.26	881	−0.18	2
5	−8.37	270.57	−0.26	1
6	−8.28	852.56	−0.39	4
Doxycycline	−7.69	2310	−0.28	3

extracts with the highest activity. The high activity of RCE may be owing to its catechin content. Similar to the extracts, (+)-catechin (FRAP = 1711.733 ± 0.956, CUPRAC = 1044.028 ± 1.039 μM TE/g) was the most potent antioxidant compound among the pure compounds. In one study, the FRAP value of (+)-catechin was found to be 8729.33 ± 424.55 mM TE/g, and in another study, it was 432.9 ± 0.94 μM Fe(II)/g [42, 43]. Except for (+)-catechin, isolated compounds showed weaker activity than extracts. In the literature, the FRAP value of euscaphic acid was recorded as 8.67 ± 3.93 mM TE/g in one study and as 31.5 ± 1.2 μM TE/g in another study [43, 44]. These results are close to the data in this study (22.067 ± 1.886 μM TE/g) and support our findings.

2.4 | Total Phenolic Contents of the Extracts

The total phenolic content of the extracts is presented in Table 2. According to the results, RCA (698.708 ± 3.680 μg GAE/mL) and RCM (639.958 ± 3.281 μg GAE/mL), which have similar values, have higher content than other extracts.

2.5 | Molecular Docking Results

Molecular docking studies were performed on both *C. histolyticum* collagenase G and *Agaricus bisporus* tyrosinase. The binding free energies of each compound were calculated for both target proteins. The grid coordinates for the collagenase G (7Z5U) structure were calculated as 40.0, −8.0, and 15.0 Å, and the grid box was set to 25 Å × 25 Å × 25 Å. Likewise, the grid box for tyrosinase (2Y9X) was set to 25 Å × 25 Å × 25 Å and the grid coordinates were calculated as −12.0 Å × −30.0 Å × −50.0 Å. Further molecular docking outputs for each compound are summarized in Tables 3 and 4. The molecular docking outputs of the studied compounds and the predicted K_i values of collagenase G inhibition are summarized in Table 3.

Among the compounds studied for collagenase inhibitory activity, euscaphic acid was identified as the most promising compound with high binding affinity to the catalytic core of *C. histolyticum* collagenase G (7Z5U) and the lowest binding free energy value of −9.12 kcal/mol. Although euscaphic acid failed to form a biochemical bond with the Zn^{+2} ion in the catalytic core, it was found to bind the catalytic core of collagenase G in a lock and key pattern and form three close hydrogen bonds with collagenase catalytic residues (Figure 2a). On the other hand, catechin has been identified as one of the most promising inhibitors of collagenase G among the compounds studied since it can potentially form four hydrogen bonds as well as a π–cation biochemical interaction with Zn^{+2} ion located at the catalytic core of collagenase G (Figure 2b). Although catechin binding free energy was the third lowest value (−8.28 kcal/mol) determined by docking studies, the estimated ligand efficient value was the highest among the studied compounds (Table 3). Moreover, 2D plot findings from the collagenase G–catechin complex illustrated that catechin is the only compound having the potential to build strong hydrogen bonds with three catalytic residues (GLY494, GLU524, and TYR599) of collagenase G. However, we could not detect such high ligand efficiency for the compound kaji-ichigoside F1 with a binding free energy of −8.81 kcal/mol. During molecular docking studies on collagenase G, doxycycline drug, a well-known collagenase inhibitor, was used as a positive control (Table 3).

Molecular docking studies performed on *C. histolyticum* collagenase G enzyme revealed that among the studied compounds, euscaphic acid and catechin reveal promising collagenase inhibition potential. Further analysis on the binding modes of both compounds revealed that their strong binding potential to collagenase enzyme can be correlated with their high potential to form hydrogen bonds with target enzyme catalytic residues.

When ligand compounds were targeted to the tyrosinase enzyme, rosamultin was found to have promising potential for binding to the active site of 2Y9X with the lowest binding free energy of −7.8 kcal/mol among the compounds studied (Figure 3a). On the other hand, kaji-ichigoside F1 and tormentic acid compounds for tyrosinase inhibition also showed promising binding affinity to the 2Y9X active site in the presence of low binding free energy values of −7.7 and 7.6 kcal/mol (Table 4). Kojic acid is a well-known inhibitor of the tyrosinase enzyme and was, therefore, used as a control molecule for the current tyrosinase enzyme molecular docking studies. In terms of ligand efficiency score, kojic acid was determined as the molecule with the highest ligand efficiency at −0.56, followed by the catechin compound at −0.33 (Table 4). Indeed, this theoretical prediction for catechin was in agreement with its low IC_{50} value obtained from the experimental results. Taking into account the parameters obtained, we further analyzed the binding mode of catechin to the 2Y9X catalytic core and determined that among the molecules studied, catechin

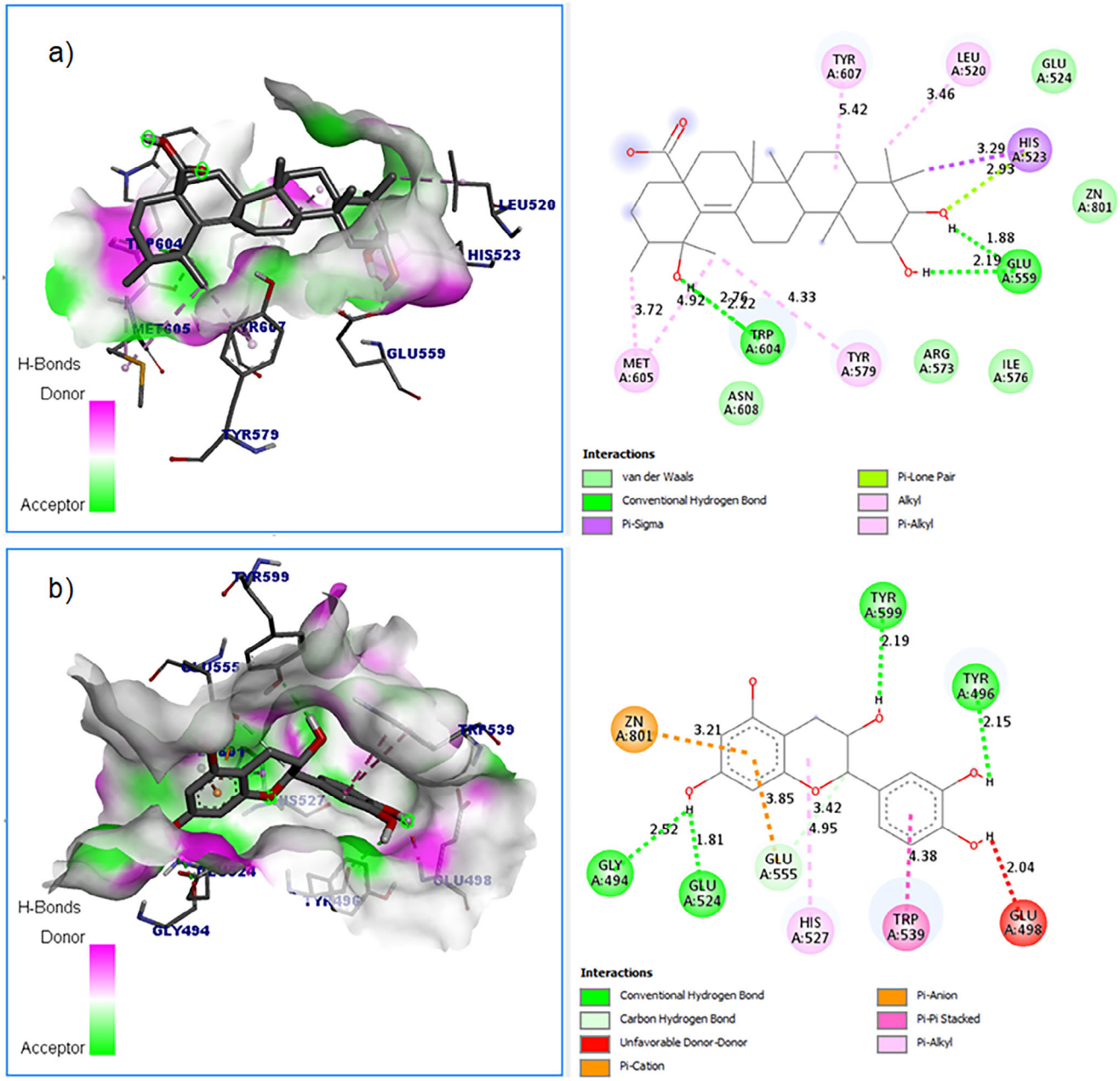

FIGURE 2 | (a) 3D visualization and 2D interaction plot of euscaphic acid–*Clostridium histolyticum* collagenase G complex. (b) 3D visualization and 2D interaction plot of catechin–*C. histolyticum* collagenase G complex. Hydrogen bonds are identified by green dashed lines.

is the only one able to form a potential metal acceptor bond with the Cu^{+2} ion positioned in the tyrosinase catalytic core (Figure 3b). Furthermore, toward better inhibitory activity, the catechin compound was able to establish two strong hydrogen bonds as well as numerous different hydrophobic interactions with the catalytic residues of the tyrosinase enzyme (Figure 3b).

Based on the molecular docking data on tyrosinase enzyme, catechin compound was found to have the highest inhibitory activity among the compounds studied. These results are consistent with the low catechin IC_{50} value obtained from previous experimental results. Taken together, current theoretical predictions suggest that catechin and its close derivatives may exhibit moderate to high inhibitory activity on both collagenase and tyrosinase enzymes.

2.6 | Pharmacokinetic Properties and Drug-Likeness of the Isolated Compounds

Cosmetic products are usually applied topically and the pharmacokinetics of the active compounds in their content are especially important in terms of skin permeability properties, efficacy, and safety [21]. The pharmacokinetic and drug-likeness properties of the isolated compounds were evaluated (Table 5). According to Lipinski's rule of five, which is evaluated for drug candidate compounds, the number of H-bond donors ≤ 5, H-bond acceptors ≤ 10, molecular weight ≤ 500 Da, and log*P* ≤ 5 for good absorption and permeability of the compounds [36]. Except for kaji-ichigoside F1 and rosamultin, other compounds meet these rules. In addition, logK_p, an important parameter for topical application, indicates skin permeability. It is a measure of the

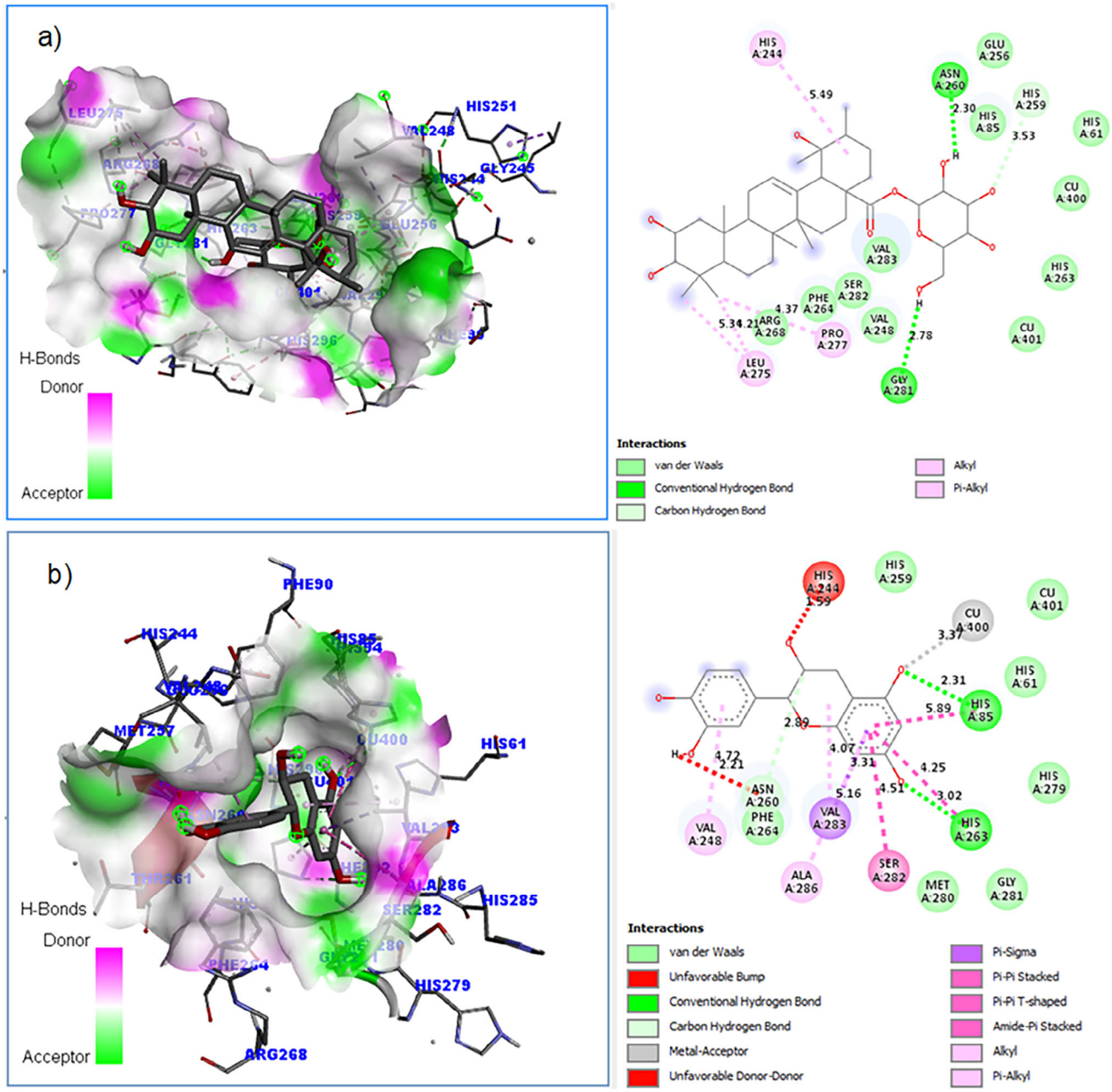

FIGURE 3 | (a) 3D visualization and 2D interaction plot of rosamultin–*Agaricus bisporus* tyrosinase enzyme complex. (b) 3D visualization and 2D interaction plot of catechin–*A. bisporus* tyrosinase enzyme complex. Hydrogen bonds are identified by green dashed lines.

ability of the compound to partition between different phases, such as the skin and the applied environment [21]. It is known that the higher the negative logK_p value, the lower the skin permeability. LogK_p < −6 indicates that the compound has low permeability. LogK_p values of euscaphic acid, tormentic acid, and 2-oxopomolic acid were found to be very close but higher than −6. Topological polar surface area (TPSA) indicates the polar surface area of the compounds and is related to their interaction with polar surfaces, such as the polar surfaces of the cell membrane. For compounds to be applied topically, a TPSA value of less than 140 Å^2 is expected [21]. Except for kaji-ichigoside F1 and rosamultin, the TPSA values of the other compounds are less than 140 Å^2. Good water solubility was found to be negatively correlated with skin permeability [21]. According to these data, euscaphic acid, tormentic acid, and 2-oxopomolic acid have moderate skin permeability and have promising drug-likeness and pharmacokinetic properties depending on the characteristics of the skin to be treated and the expected effect. Catechin, which showed significant activity in in vitro and in silico studies, has poor skin permeability. This problem can be overcome by preparing modern topical formulations to increase the skin permeability of these compounds.

3 | Conclusions

The inhibition of enzymes that degrade the extracellular matrix and the enhancement of the skin's antioxidant defense

TABLE 4 | Molecular docking outputs of the studied compounds and predicted K_i values of tyrosinase inhibition.

Ligand ID	2Y9X Binding energy (kcal/mol)	Estimated K_i (μM)	Ligand efficiency	H bond
1	−7.3	4.46	−0.21	1
2	−7.6	2.69	−0.22	1
3	−7.7	2,27	−0.17	1
4	−7.8	1.92	−0.17	2
5	−7.4	3.77	−0.21	2
6	−7.1	7.40	−0.33	2
Kojic acid	−5.6	78.56	−0.56	1

TABLE 5 | Pharmacokinetic properties and drug-likeness of the isolated compounds.

Ligand	Molecular weight (g/mol)	nHBD	nHBA	Solubility[a]			Lipophilicity[b]	TPSA (Å²)	logK_p
				log*S* (ESOL)	log*S* (Ali)	log*S* (SILICOS-IT)			
1	488.70	4	5	M	P	M	4.30	97.99	−5.76 cm/s
2	488.70	4	5	M	P	M	4.40	97.99	−5.76 cm/s
3	650.84	7	10	M	P	S	2.62	177.14	−8.03 cm/s
4	650.84	7	10	M	P	S	2.54	177.14	−8.03 cm/s
5	486.68	3	5	M	P	M	4.39	94.83	−5.75 cm/s
6	290.27	5	6	S	S	S	0.85	110.38	−7.82 cm/s

Abbreviations: logK_p, skin permeation of compounds (cm/s); nHBA, number of hydrogen bond acceptor; nHBD, number of hydrogen bond donor; TPSA, topological polar surface area.

[a]S, soluble; M, moderately soluble; P, poorly soluble.

[b]Lipophilicity was represented according to the average of all five log$P_{o/w}$ predictions.

mechanism are important approaches to prevent skin aging. *R. canina* is a plant with important pharmacological effects that is widely distributed worldwide and in Türkiye. In this study, anti-collagenase, anti-tyrosinase, and antioxidant activities of the extracts prepared from its roots and isolated compounds were revealed. In addition, the pharmacokinetic and drug-likeness properties of the isolated compounds were also evaluated. Compounds isolated from their roots for the first time, especially (+)-catechin, stand out in their important anti-collagenase and anti-tyrosinase activities. The active extracts and compounds have remarkable potential for the development of cosmetic products with antiaging, anti-wrinkle, and skin-whitening properties. For cosmetic use of these compounds, appropriate topical formulations should be prepared to increase their skin permeability. Our findings have revealed that the roots of *R. canina* are a valuable source of bioactive compounds, especially (+)-catechin, with precious cosmetic effects. These results provide a scientific basis for further studies (in vivo, clinical, and toxicological studies) and industrial use of the plant.

4 | Experimental Section

4.1 | Collection and Identification of the Plant

The roots of *R. canina* were collected from Kafkasor, Artvin, Türkiye (41°9′55″ N, 41°47′47″ E, 1210 m) in July 2023. The authentication of the plant material was performed by the authors, Prof. Ufuk Özgen and Prof. Özgür Eminağaoğlu. The voucher specimen (KATO19488) was deposited at the Karadeniz Technical University, Faculty of Forestry Herbarium in Trabzon, Türkiye. The roots were washed and dried in the shade, then cut into small pieces and ground into fine powder.

4.2 | Extraction, Fractionation, and Isolation Procedures

The finely powdered roots (500 g) were extracted with methanol (2 L) using a shaker (Heidolph Unimax 1010) at room temperature, and then the extract was filtrated. This process was done twice, and the final filtrates were combined. The combined extracts were evaporated to dryness under a vacuum using a rotary evaporator (Heidolph Hei-VAP Precision) at 40°C, and RCM was obtained (yield: 15%). The crude extract was dissolved in MeOH:H_2O 9:1 (300 mL), and successively extracted with chloroform (2 × 300 mL) and ethyl acetate (2 × 300 mL) using a liquid–liquid extraction method. The solvent extracts were concentrated by evaporation under vacuum to give RCC (yield: 29.2%) and RCE (yield: 10.3%), respectively. Then, the remaining aqueous phase was evaporated to dryness to give RCA (yield: 47.9%).

Following fractionation procedures, RCC (20 g) was chromatographed over silica gel column chromatography (Kieselgel 60, 0.040–0.063 mm, 40 × 4 cm) eluted with *n*-hexane:EtOAc (9:1, 8:2, 7:3, 5:5 and 0:10, respectively). Fractions (A, 10 mL) were collected, and 195 fractions were obtained. Depending on thin-layer chromatography (TLC; Silica gel, 60 F_{254}) profiles, Fractions A83-169 (1 g) were combined and subjected to a silica gel column (Kieselgel 60, 0.040–0.063 mm, 40 × 2.5 cm). *n*-Hexane:EtOAc (9:1, 8:2, 7:3, 5:5, and 0:10, respectively) solvent systems were used as eluents and Fractions A133-156 (0.5 g) were united. The combined fractions were applied to a silica gel column (Kieselgel 60, 0.040–0.063 mm, 40 × 2.5 cm) using a gradient elution with *n*-hexane:EtOAc (0:100 → 100:0), 202 Fractions (B) were obtained and Fraction B59 gave compound **1** (15.2 mg). In addition, Fractions A190-193 were combined to yield compound **2** (12 mg).

RCE (6.5 g) was subjected to Sephadex LH-20 (Sigma, USA) column chromatography (30 × 2.5 cm) in three parts eluted with MeOH 100%. Based on TLC, Fractions 4–8 of the columns were combined and chromatographed over vacuum liquid chromatography on reverse phase silica gel (LiChroprep RP-18 25-40 μm, 45 × 3 cm) eluting with a gradient mixture of H_2O:MeOH (100:0 → 0:100) and fractions were collected in 20 mL. Fractions 122–130 (0.5 g) were applied to a silica gel column (Kieselgel 60, 0.040–0.063 mm, 45 × 2.5 cm) eluted with $CHCl_3$:MeOH:H_2O (90:10:1 → 80:20:2) and Fraction 24 led to the isolation of compound **3** (85 mg). During this column, Fraction 133 gave compound **4** (72 mg). Fractions 160–171 of the column (400 mg) were chromatographed over on silica gel (Kieselgel 60, 0.040–0.063 mm, 40 × 2.5 cm, volumes of 10 mL) and $CHCl_3$:MeOH:H_2O (90:10:1 → 80:20:2) solvent systems was used as eluent. According to TLC profiles, Fractions 4–7 of the column were combined to yield compound **5** (15 mg). Fractions 9–13 of the Sephadex column were combined and subjected to a silica gel column (Kieselgel 60, 0.040–0.063 mm, 45 × 2.5 cm, volumes of 10 mL) eluting with $CHCl_3$:MeOH:H_2O (90:10:1 → 50:50:5). Fraction 20 of the column gave compound **6** (20 mg).

4.3 | Elucidation of Structures of the Isolated Compounds

The chemical structures of the isolated compounds were elucidated by 1D (^{1}H-NMR and ^{13}C-NMR) and 2D NMR (COSY, HMBC HSQC, and NOESY) techniques. The compounds were analyzed by dissolving them in deuterated methanol (CD_3OD) and NMR spectra have been obtained by Bruker Ascend 400 MHz/54 mm ULH. NMR spectra of the compounds are given as Supporting Information. Polarimetry was used to determine the structure of **6**.

4.4 | Enzyme Inhibition Assays

The collagenase enzyme inhibition was determined spectrophotometrically using a modified method [45]. *C. histolyticum* collagenase (Type I, EC 3.4.24.3, Sigma, USA, 0.8 U/mL) was used as the enzyme source, and N-[3-(2-Furyl)acryloyl]-Leu-Gly-Pro-Ala (FALGPA) solution (2 mM) as a substrate. The enzyme, substrate, extracts, and compounds (**1–5**) (6.125–400 μg/mL) were dissolved in 50 mM Tris-HCl buffer (0.4 M NaCl and 0.01 M $CaCl_2$, pH 7.5). Catechin (3.125–200 μg/mL) was used as a positive control. The samples' absorbance was read on the microplate reader (BMG Labtech Spectrostar Nano) at 340 nm. The tyrosinase inhibition was examined by the method modified by Likhitwitayawuid and Sritularak [46], using 3,4-dihydroxy-L-phenylalanine (L-DOPA) as a substrate. The samples and α-kojic acid, used as a positive control, were prepared at different concentrations

(6.125–500 μg/mL) using potassium phosphate buffer (pH 6.8). Mushroom tyrosinase (EC 1.14.18.1, Sigma, USA, 46 units/mL) was used as an enzyme. End of the procedure, the absorbance of the samples was read on a microplate reader at 490 nm. By taking the mean of the results obtained, the percentage inhibition values were calculated based on the formula given below.

$$\text{Enzyme inhibition } (\%) = [(A - B) - (C - D)] / (A - B) \times 100$$

where A is the absorbance of negative control, B is the absorbance of negative control blank, C is the absorbance of sample, and D is the absorbance of a blank.

4.5 | Antioxidant Activity Assays

The antioxidant capacities of the extracts and compounds were determined using FRAP and CUPRAC assays. The principle of these assays is based on spectrophotometric measurement of Fe^{+3} and Cu^{+2} reducing capacities of the samples, respectively [47, 48]. In both assay, Trolox, used as standard, was prepared at different concentrations (1000–62.5 μM). The absorbance of the samples was read at 595 and 450 nm, respectively. The antioxidant capacities of the samples were compared with Trolox and expressed as μM TEAC/g sample.

4.6 | Total Phenolic Content of the Extracts

The total soluble phenolic substance amount of the extracts was determined using the method by Slinkard and Singleton [49]. The absorbances were read at 765 nm by spectrophotometer. Gallic acid was used as a standard and the total phenolic content of the extracts was expressed as μg gallic acid equivalents (GAE)/mL.

4.7 | In Silico Assays

4.7.1 | Molecular Docking

Molecular docking studies were performed on two different protein targets: *C. histolyticum* (synonym: *Hathewaya histolytica*) collagenase G (Type I, EC 3.4.24.3) and *A. bisporus* tyrosinase. Collagenase G enzyme contains one Zn^{+2} ion bound to its catalytic core [50]. Thus, molecular docking studies on collagenase G were performed using the AutoDockZN program [51]. On the other hand, molecular docking studies on the tyrosinase target (2Y9X) containing two Cu^{+2} ions bound to its active site as cofactors were performed using the AutoDockVina program (Version 1.5.7). Three-dimensional (3D) structures of *C. histolyticum* collagenase G (PDB ID: 7Z5U, resolution: 1.8 Å) and *A. bisporus* tyrosinase (PDB ID: 2Y9X, resolution: 2.78 Å) [52] were retrieved from the Protein Data Bank (www.rcsb.org). Three of the four subunits (chain B, C, and D) were removed from the tetrameric crystal structure of 2Y9X using PyMOL (The PyMOL Molecular Graphics System, Version 2.0 Schrödinger, LLC). Except for two Cu^{+2} ions bound to the 2Y9X active site, the bound tropolone inhibitor and water molecules were then deleted using the AutoDockTools program [53]. The biochemical interaction of the synthesized compounds with Cu^{+2} ions was monitored during docking studies. Based on the pK_a values and the pH of the system, ionizable residues in the protein structure were protonated using PROPKA3.1 [54]. Missing residue detection and correction processes and following energy minimization were applied to eliminate any steric clashes on the target protein and optimize its geometry. The tropolone binding site in the 3D structure of 2Y9X was used as a reference to properly define the grid box center and grid box dimensions using the AutoGrid4 program [53].

The pdb files of the ligand compounds were prepared using the OpenBabel program and then converted to pdbqt files for use in docking studies. Using the ligand pdbqt files, each docking experiment was performed in two independent runs. The docking outputs were then examined in detail, and specific 2D interaction maps for ligand compounds with high inhibition potential were analyzed using Discovery Studio Accelrys (v21.1.0.20298) (Discovery Studio Visualizer) program (Dassault Systems, BIOVIA). Following molecular docking studies, the ligand efficiency value (LE) for each compound was calculated by taking the ratio of the binding free energy value (ΔG) to the number of heavy (non-hydrogen) atoms (HA) of the ligand. Compounds with LE values > 0.3 were considered as potential lead compounds (ΔG/HA) [55].

4.7.2 | Assessment of Pharmacokinetic and Drug-Likeness Properties

The SwissADME server is used to assess the pharmacokinetic and drug-likeness properties of the compounds in silico. The SMILES of the compounds obtained by drawing the chemical formulas of them were used in the analysis. Using this server, physicochemical properties (water solubility, TPSA), lipophilicity, pharmacokinetic properties such as skin permeability ($\log K_p$), and drug-likeness properties were evaluated according to the Lipinski's rules of five [56].

4.8 | Statistical Analysis

In the in vitro studies, each sample was studied in triplicate. In the enzyme inhibition assays, IC_{50} values of the samples were found with the help of the graph drawn with the calculated percentage inhibition data and the logarithmic concentrations of the samples using Microsoft Excel. Graphs regarding enzyme inhibition are provided as Supporting Information. Experimental results were given as means ± standard deviation (SD).

Author Contributions

Tuğba Subaş: writing – original draft, methodology, validation, investigation, visualization, data curation. **Ufuk Özgen**: conceptualization, methodology, supervision, writing – review and editing, project administration, funding acquisition. **Şeyda Kanbolat**: writing – original draft, methodology, validation, investigation, visualization, data curation. **Merve Badem**: writing – original draft, methodology, validation, investigation, visualization, data curation. **Uğur Uzuner**: investigation, visualization, writing – original draft, data curation, resources. **Gonca Özdemir**: investigation, funding acquisition. **Şule Zeytineli**: investigation. **Şeyma Altunışık**: investigation. **Halide Cangul**: investigation. **Özgür Eminağaoğlu**: resources.

Acknowledgments

This research was funded by a grant of The Scientific and Technological Research Council of Türkiye (TUBITAK) (grant number: 1919B012337704) and Office of Scientific Research Projects of Karadeniz Technical University (grant number: TLÖ-2023-11098). The authors gratefully acknowledge Prof. Dr. Hasan Seçen for his valuable contribution to the interpretation of the NOESY spectra and the elucidation of the stereochemical configurations of the compounds.

Conflicts of Interest

The authors declare no conflict of interest.

Data Availability Statement

The data that support the findings of this study are available in the Supporting Information of this article.

References

1. A. Güner, S. Aslan, T. Ekim, M. Vural, and M. T. Babaç, "Türkiye Bitkileri Listesi (Damarlı Bitkiler)," in *Türkiye Bitkileri Listesi*, ed. A. Güner, S. Aslan, T. Ekim, M. Vural, and M. T. Babaç (Nezahat Gökyiğit Botanik Bahçesi Ve Flora Araştırmaları Derneği Yayını, 2012).

2. Plants of the World Online, "*Rosa* L.," accessed August 1, 2024, https://powo.science.kew.org/taxon/urn:lsid:ipni.org:names:30002432-2.

3. M. Oz, C. Baltaci, and I. Deniz, "Gümüşhane Yöresi Kuşburnu (*Rosa canina* L.) ve Siyah Kuşburnu (*Rosa pimpinellifolia* L.) Meyvelerinin C Vitamini ve Şeker Analizleri," *Gümüşhane Üniversitesi Fen Bilimleri Dergisi* 8, no. 2 (2018): 284–292.

4. M. Khazaei, M. R. Khazaei, and M. Pazhouhi, "An Overview of Therapeutic Potentials of *Rosa canina*: A Traditionally Valuable Herb," *World Cancer Research Journal* 7 (2020): e1580.

5. E. Altundag and M. Ozturk, "Ethnomedicinal Studies on the Plant Resources of East Anatolia, Turkey," *Procedia—Social and Behavioral Sciences* 19 (2011): 756–777.

6. M. Macit, A. Aras, E. Çapanoğlu Güven, and S. Bakir, "Investigating the Content and Bioaccessibility of Phenolic Compounds in Roots of *Rosa canina* L. and *Rosa pimpinellifolia* L.," *Yüzüncü Yıl Üniversitesi Tarım Bilimleri Dergisi* 33, no. 2 (2023): 163–173.

7. D. Deliorman Orhan, B. Ozçelik, S. Hoşbaş, and M. Vural, "Assessment of Antioxidant, Antibacterial, Antimycobacterial, and Antifungal Activities of Some Plants Used as Folk Remedies in Turkey against Dermatophytes and Yeast-Like Fungi," *Turkish Journal of Biology* 36 (2012): 672–686.

8. N. V. Anil Kumar, C. Quispe, J. Herrera-Bravo, et al., "Potential of Mushrooms Bioactive for the Treatment of Skin Diseases and Disorders," *Journal of Food Biochemistry* 2023 (2023): 5915769.

9. M. Chatatikun and A. Chiabchalard, "Thai Plants With High Antioxidant Levels, Free Radical Scavenging Activity, Anti-Tyrosinase and Anti-Collagenase Activity," *BMC Complementary and Alternative Medicine* 17, no. 1 (2017): 487.

10. I. Chiocchio, M. Mandrone, C. Sanna, A. Maxia, M. Tacchini, and F. Poli, "Screening of a Hundred Plant Extracts as Tyrosinase and Elastase Inhibitors, Two Enzymatic Targets of Cosmetic Interest," *Industrial Crops and Products* 122 (2018): 498–505.

11. K E. Lee, S. Bharadwaj, U. Yadava, and S. Gu Kang, "Evaluation of Caffeine as Inhibitor against Collagenase, Elastase and Tyrosinase Using *In Silico* and *In Vitro* Approach," *Journal of Enzyme Inhibition and Medicinal Chemistry* 34, no. 1 (2019): 927–936.

12. F. S. Senol Deniz, R. E. Salmas, E. Emerce, I. I. T. Cankaya, H. S. Yusufoglu, and I. Erdogan Orhan, "Evaluation of Collagenase, Elastase and Tyrosinase Inhibitory Activities of *Cotinus coggygria* Scop. Through *In Vitro* and *In Silico* Approaches," *South African Journal of Botany* 132 (2020): 277–288.

13. J. N. Manjia, E. M. Njoya, A. Harishchander, et al., "Anti-Elastase, Anti-Tyrosinase, and Anti-Inflammatory Activities of Three Compounds Isolated From *Psorospermum aurantiacum*: *In Silico* and *In Vitro* Assays," *Revista Brasileira de Farmacognosia* 34, no. 5 (2024): 1116–1128.

14. P. Limtrakul, S. Yodkeeree, P. Thippraphan, W. Punfa, and J. Srisomboon, "Anti-Aging and Tyrosinase Inhibition Effects of *Cassia fistula* Flower Butanolic Extract," *BMC Complementary and Alternative Medicine* 16, no. 1 (2016): 497.

15. F. S. Senol Deniz, I. E. Orhan, and H. Duman, "Profiling Cosmeceutical Effects of Various Herbal Extracts Through Elastase, Collagenase, Tyrosinase Inhibitory and Antioxidant Assays," *Phytochemistry Letters* 45 (2021): 171–183.

16. H. Mechqoq, S. Hourfane, M. El Yaagoubi, et al., "Molecular Docking, Tyrosinase, Collagenase, and Elastase Inhibition Activities of Argan By-Products," *Cosmetics* 9, no. 1 (2022): 24.

17. P. Srisuksomwong, L. Kaenhin, and L. Mungmai, "Collagenase and Tyrosinase Inhibitory Activities and Stability of Facial Cream Formulation Containing Cashew Leaf Extract," *Cosmetics* 10, no. 1 (2023): 17.

18. J. Bae, N. Kim, Y. Shin, S. Y. Kim, and Y. J. Kim, "Activity of Catechins and Their Applications," *Biomedical Dermatology* 4 (2020): 8.

19. M. Maghsoudloo, R. Bagheri Shahzadeh Aliakbari, and Z. Jabbari Velisdeh, "Pharmaceutical, Nutritional, and Cosmetic Potentials of Saponins and Their Derivatives," *Nano Micro Biosystems* 2, no. 4 (2023): 1–6.

20. J. K. Liu, "Natural Products in Cosmetics," *Natural Products and Bioprospecting* 12, no. 1 (2022): 40.

21. M. Hammami, E. Chaabani, W. Yeddes, W. Aidi Wannes, and S. Bourgou, "Phenolic Compounds and Skin Permeability: An *In Silico* Investigation," *Avicenna Journal of Medical Biochemistry* 11, no. 1 (2023): 11–18.

22. Y. Wang, Y. Zhao, X. Liu, J. Li, J. Zhang, and D. Liu, "Chemical Constituents and Pharmacological Activities of Medicinal Plants From *Rosa* Genus," *Chinese Herbal Medicines* 14, no. 2 (2022): 187–209.

23. G. de Graça Rocha, M. Simões, K. A. Lúcio, R. R. Oliveira, M. A. C. Kaplan, and C. R. Gattass, "Natural Triterpenoids From *Cecropia lyratiloba* Are Cytotoxic to Both Sensitive and Multidrug Resistant Leukemia Cell Lines," *Bioorganic & Medicinal Chemistry* 15, no. 23 (2007): 7355–7360.

24. L. Guven, U. Ozgen, H. Secen, et al., "Phytochemical Studies on the Seeds, Pseudofruits, and Roots of *Rosa pimpinellifolia*," *Journal of Research in Pharmacy* 25, no. 2 (2021): 153–163.

25. N. Y. Song, J. G. Cho, D. Im, et al., "Triterpenoids From *Fragaria ananassa* Calyx and Their Inhibitory Effects on Melanogenesis in B16-F10 Mouse Melanoma Cells," *Natural Product Research* 27, no. 23 (2013): 2219–2223.

26. N. Coruh and N. Ozdogan, "Wild-Growing *Rosa heckeliana* Tratt.: Phenolic Constituents with Cytotoxic and Antioxidative Properties," *Turkish Journal of Biology* 41 (2017): 195–212.

27. H. J. Jung, J. H. Nam, J. Choi, K. T. Lee, and H. J. Park, "19α-Hydroxyursane-Type Triterpenoids: Antinociceptive Anti-Inflammatory Principles of the Roots of *Rosa rugosa*," *Biological and Pharmaceutical Bulletin* 28, no. 1 (2005): 101–104.

28. H. N. Dai, G. X. Ma, J. M. Zhou, et al., "Triterpenoids From Roots of *Rosa laevigata*," *Zhongguo Zhong Yao Za Zhi* 41, no. 12 (2016): 2267–2272.

29. X. Fan, L. Bai, L. Lin, et al., "Studies on the Chemical Constituents and Quality Evaluation of *Rosa cymosa* Tratt. Root," *Journal of Separation Science* 43, no. 24 (2020): 4379–4389.

30. Q. J. Li, Y. Nan, J. J. Qin, Y. Yang, X. J. Hao, and X. S. Yang, "Chemical Constituents From Medical and Edible Plants of *Rosa roxburghii*," *Zhongguo Zhong Yao Za Zhi* 41, no. 3 (2016): 451–455.

31. O. Taofiq, A. M. González-Paramás, M. F. Barreiro, and I. C. Ferreira, "Hydroxycinnamic Acids and Their Derivatives: Cosmeceutical

Significance, Challenges and Future Perspectives, a Review," *Molecules* 22, no. 2 (2017): 281.

32. Y. H. Hong, E. Y. Jung, D. O. Noh, and H. J. Suh, "Physiological Effects of Formulation Containing Tannase-Converted Green Tea Extract on Skin Care: Physical Stability, Collagenase, Elastase, and Tyrosinase Activities," *Integrative Medicine Research* 3, no. 1 (2014): 25–33.

33. T. S. Thring, P. Hili, and D. P. Naughto, "Anti-Collagenase, Anti-Elastase and Anti-Oxidant Activities of Extracts From 21 Plants," *BMC Complementary and Alternative Medicine* 9 (2009): 27.

34. J. M. Andrade, E. M. Domínguez-Martín, M. Nicolai, C. Faustino, L. M. Rodrigue, and P. Rijo, "Screening the Dermatological Potential of *Plectranthus* Species Components: Antioxidant and Inhibitory Capacities Over Elastase, Collagenase and Tyrosinase," *Journal of Enzyme Inhibition and Medicinal Chemistry* 36, no. 1 (2021): 258–270.

35. B. Madhan, G. Krishnamoorthy, J. R. Rao, and B. U. Nair, "Role of Green Tea Polyphenols in the Inhibition of Collagenolytic Activity by Collagenase," *International Journal of Biological Macromolecules* 41, no. 1 (2007): 16–22.

36. B. H. Abbasi, A. Siddiquah, D. Tungmunnithum, et al., "*Isodon rugosus* (Wall. ex Benth.) Codd *In Vitro* Cultures: Establishment, Phytochemical Characterization and *In Vitro* Antioxidant and Anti-Aging Activities," *International Journal of Molecular Sciences* 20, no. 2 (2019): 452.

37. Z. Tohtahon, L. Zhang, J. Han, X. Xie, Z. Tu, and T. Yuan, "Extraction Optimization, Structural Characterization and Bioactivity Evaluation of Triterpenoids From Hawthorn (*Crataegus cuneata*) Fruits," *Journal of Food Biochemistry* 41, no. 4 (2017): e12377.

38. B. S. Liu, J. E. Ki, and N. H. Lee, "Whitening and Anti-Oxidative Activities of Chemical Components Extracted From Branches of *Sorbus alnifolia*," *Journal of the Korean Chemical Society* 67, no. 2 (2023): 137–144.

39. H. Tan, T. Sonam, and K. Shimizu, "The Potential of Triterpenoids from Loquat Leaves (*Eriobotrya japonica*) for Prevention and Treatment of Skin Disorder," *International Journal of Molecular Sciences* 18, no. 5 (2017): 1030.

40. F. Ullah, H. Hussain, J. Hussain, et al., "Tyrosinase Inhibitory Pentacyclic Triterpenes and Analgesic and Spasmolytic Activities of Methanol Extracts of *Rhododendron collettianum*," *Phytotherapy Research* 21, no. 11 (2007): 1076–1081.

41. D. Stojiljković, D. Pavlović, and I. Arsić, "Oxidative Stress, Skin Aging and Antioxidant Therapy," *Acta Facultatis Medicae Naissensis* 31, no. 4 (2014): 207–217.

42. J. H. Liang, H. R. Lin, C. S. Yang, C. C. Liaw, I. C. Wang, and J. J. Chen, "Bioactive Components From *Ampelopsis japonica* With Antioxidant, Anti-α-Glucosidase, and Antiacetylcholinesterase Activities," *Antioxidants* 11, no. 7 (2022): 1228.

43. T. Afsar, S. Razak, M. Shabbir, and M. R. Khan, "Antioxidant Activity of Polyphenolic Compounds Isolated From Ethyl-Acetate Fraction of *Acacia hydaspica* R. Parker," *Chemistry Central Journal* 12, no. 1 (2018): 5.

44. X. Li, W. Cao, Y. Shen, et al., "Antioxidant Compounds From *Rosa laevigata* Fruits," *Food Chemistry* 130, no. 3 (2012): 575–580.

45. E. Küpeli Akkol, I. Süntar, M. Ilhan, and E. Aras, "*In Vitro* Enzyme Inhibitory Effects of *Rubus sanctus* Schreber and Its Active Metabolite as a Function of Wound Healing Activity," *Journal of Herbal Medicine* 5, no. 4 (2015): 207–210.

46. K. Likhitwitayawuid and B. Sritularak, "A New Dimeric Stilbene with Tyrosinase Inhibitiory Activity From *Artocarpus gomezianus*," *Journal of Natural Products* 64, no. 11 (2001): 1457–1459.

47. I. F. Benzie and J. J. Strain, "Ferric Reducing/Antioxidant Power Assay: Direct Measure of Total Antioxidant Activity of Biological Fluids and Modified Version for Simultaneous Measurement of Total Antioxidant Power and Ascorbic Acid Concentration," *Methods in Enzymology* 299 (1999): 15–27.

48. R. Apak, K. Güçlü, B. Demirata, et al., "Comparative Evaluation of Various Total Antioxidant Capacity Assays Applied to Phenolic Compounds With the CUPRAC Assay," *Molecules* 12, no. 7 (2007): 1496–1547.

49. K. Slinkard and V. L. Singleton, "Total Phenol Analysis: Automation and Comparison with Manual Methods," *American Journal of Enology and Viticulture* 28, no. 1 (1977): 49–55.

50. U. Eckhard, E. Schönauer, and H. Brandstetter, "Structural Basis for Activity Regulation and Substrate Preference of Clostridial Collagenases G, H, and T," *Journal of Biological Chemistry* 288, no. 28 (2013): 20184–20194.

51. D. Santos-Martins, S. Forli, M. J. Ramos, and A. J. Olson, "AutoDock4$_{Zn}$: An Improved AutoDock Force Field for Small-Molecule Docking to Zinc Metalloproteins," *Journal of Chemical Information and Modeling* 54, no. 8 (2014): 2371–2379.

52. W. T. Ismaya, H. J. Rozeboom, A. Weijn, et al., "Crystal Structure of *Agaricus bisporus* Mushroom Tyrosinase: Identity of the Tetramer Subunits and Interaction With Tropolone," *Biochemistry* 50, no. 24 (2011): 5477–5486.

53. G. M. Morris, R. Huey, W. Lindstrom, et al., "AutoDock4 and AutoDockTools4: Automated Docking With Selective Receptor Flexibility," *Journal of Computational Chemistry* 30, no. 16 (2009): 2785–2791.

54. M. H. Olsson, C. R. Søndergaard, M. Rostkowski, and J. H. Jensen, "PROPKA3: Consistent Treatment of Internal and Surface Residues in Empirical pK_a Predictions," *Journal of Chemical Theory and Computation* 7, no. 2 (2011): 525–537.

55. P. W. Kenny, "The Nature of Ligand Efficiency," *Journal of Cheminformatics* 11, no. 1 (2019): 8.

56. A. Kumari, R. Kumar, G. Sulabh, et al., "*In Silico* ADMET, Molecular Docking and Molecular Simulation-Based Study of Glabridin's Natural and Semisynthetic Derivatives as Potential Tyrosinase Inhibitors," *Advances in Traditional Medicine* 23, no. 3 (2023): 733–751.

Supporting Information

Additional supporting information can be found online in the Supporting Information section.

Supporting Fig. 1: 1H-NMR of Euscaphic acid (400 MHz, CD3OD). **Supporting Fig. 2**: 13C-NMR of Euscaphic acid (100 MHz, CD3OD)/ **Supporting Fig. 3**: 13C-NMR-II of Euscaphic acid (100 MHz, CD3OD). **Supporting Fig. 4**: COSY spectrum of Euscaphic acid. **Supporting Fig. 5**: HMBC spectrum of Euscaphic acid. **Supporting Fig. 6**: HMBC spectrum II of Euscaphic acid. **Supporting Fig. 7**: HSQC spectrum of Euscaphic acid. **Supporting Fig. 8**: HSQC spectrum II of Euscaphic acid. **Supporting Fig. 9**: NOESY spectrum of Euscaphic acid. **Supporting Fig. 10**: 1H-NMR of Tormentic acid (400 MHz, CD3OD). **Supporting Fig. 11**: 13C-NMR of Tormentic acid (100 MHz, CD3OD). **Supporting Fig. 12**: 13C-NMR II of Tormentic acid (100 MHz, CD3OD). **Supporting Fig. 13**: COSY spectrum of Tormentic acid. **Supporting Fig. 14**: HMBC spectrum of Tormentic acid. **Supporting Fig. 15**: HMBC spectrum II of Tormentic acid. **Supporting Fig. 16**: HSQC spectrum of Tormentic acid. **Supporting Fig. 17**: NOESY spectrum of Tormentic acid. **Supporting Fig. 18**: 1H-NMR of Kaji-ichigoside F1 (400 MHz, CD3OD). **Supporting Fig. 19**: 13C-NMR of Kaji-ichigoside F1 (100 MHz, CD3OD). **Supporting Fig. 20**: 13C-NMR II of Kaji-ichigoside F1 (100 MHz, CD3OD). **Supporting Fig. 21**: COSY spectrum of Kaji-ichigoside F1. **Supporting Fig. 22**: HMBC spectrum of Kaji-ichigoside F1. **Supporting Fig. 23**: HSQC spectrum of Kaji-ichigoside F1. **Supporting Fig. 24**: NOESY spectrum of Kaji-ichigoside F1. **Supporting Fig. 25**: 1H-NMR spectrum of Rosamultin (400 MHz, CD3OD). **Supporting Fig. 26**: 13C-NMR spectrum of Rosamultin (100 MHz, CD3OD). **Supporting Fig. 27**: 13C-NMR II spectrum of Rosamultin (100 MHz, CD3OD). **Supporting Fig. 28**: COSY spectrum of Rosamultin. **Supporting Fig. 29**: HSQC spectrum

of Rosamultin. **Supporting Fig. 30**: NOESY spectrum of Rosamultin. **Supporting Fig. 31**: 1H-NMR of 2-oxopomolic acid (400 MHz, CD3OD). **Supporting Fig. 32**: 13C-NMR of 2-oxopomolic acid (100 MHz, CD3OD). **Supporting Fig. 33**: 13C-NMR II of 2-oxopomolic acid (100 MHz, CD3OD). **Supporting Fig. 34**: COSY spectrum of 2-oxopomolic acid. **Supporting Fig. 35**: HMBC spectrum of 2-oxopomolic acid. **Supporting Fig. 36**: HSQC spectrum of 2-oxopomolic acid. **Supporting Fig. 37**: NOESY spectrum of 2-oxopomolic acid. **Supporting Fig. 38**: 1H-NMR spectrum of (+)-catechin (400 MHz, CD3OD). **Supporting Fig. 39**: 13C-NMR spectrum of (+)-catechin (100 MHz, CD3OD). **Supporting Fig. 40**: Graphs related to tyrosinase enzyme inhibition. **Supporting Fig. 41**: Graphs related to tyrosinase enzyme inhibition II. **Supporting Fig. 42**: Graphs related to collagenase enzyme inhibition. **Supporting Fig. 43**: Graphs related to collagenase enzyme inhibition II. **Supporting Table 1**: 1H-NMR data (CD3OD) of compounds **1**-**5**. **Supporting Table 2**: 13C-NMR data (CD3OD) of compounds **1**-**5**. **Supporting Table 3**: 1H and 13C-NMR data (CD3OD) of compound **6**.